Gas-particle partitioning and air-water exchange of polycyclic aromatic hydrocarbons in the Three Gorges Reservoir, southwest China

Fengwen Wang[ac*], Daiyin Zhao[c], Siyuan Zhang[c], Ting Feng[c], Haoqi Wang[c], Zhigang Guo[d], Lei Ma[ab*], Neil L. Rose[e]

[a]Observation and Research Station of Ecological Restoration for Chongqing Typical Mining Areas, Ministry of Natural Resources, Chongqing Institute of Geology and Mineral Resources, 401120, China

[b]College of Resources and Safety Engineering, Chongqing University, Chongqing 400030, China

[c]Key Laboratory of the Three Gorges Reservoir Region' s Eco-Environment, Ministry of Education, Department of Environmental Science, Chongqing University, Chongqing, 400030, China

[d]Shanghai Key Laboratory of Atmospheric Particle Pollution and Prevention, Center for Atmospheric Chemistry Study, Department of Environmental Science and Engineering, Fudan University, Shanghai 200433, China

[e]Environmental Change Research Centre, University College London, Gower Street, London WC1E 6BT, United Kingdom

[*]Corresponding author: fengwenwang@cqu.edu.cn (Wang F.)

13953057@qq.com (Ma L.)

Abstract:

A 30 m vertical drawdown water level fluctuation zone (WLFZ) was formed annually due to seasonal water impoundment in the Three Gorges Reservoir (TGR) in

Southwest China. In this study, a super site in downstream of WLFZ, ~ 200 km off the Three Gorges Dam, was used to investigate the seasonally gas-particle partitioning and air-water exchange of USEPA 16 polycyclic aromatic hydrocarbons (16 PAHs). The average concentrations of 16 PAHs in the particle phase were 66.63±9.15 ng/m^3 in winter and 8.43±2.95 ng/m^3 in summer. In the gas phase, they were 28.47±4.79 ng/m^3 in winter and 10.57±1.51 ng/m^3 in summer. In the dissolved phase of surface water, they were 38.65±6.37 ng/L in winter and 56.53±8.86 ng/L in summer. The logarithmic gas-particle partitioning coefficient (lgK_p) was negatively correlated with the logarithmic subcooled liquid vapor pressure (lgP_L^0). While the lgK_p was positively correlated with logarithmic octanol-air distribution coefficient (lgK_{OA}). These two regressions both indicated un-equilibrium of gas-particle partitioning of PAHs in the atmosphere. Applying "Whitman two-film resistance model" to our datasets shows that 3-ring PAHs had a net volatilization from water to air (2.74 to 6.43 ng/m^2/d), and 4~5-ring PAHs favored deposition from air to water (-0.614 to -0.413 ng/m^2/d). The water as a potential 'source' for 3-ring and a 'sink' for 4~5-ring PAHs was thereby revealed. The results of this study are crucial for understanding atmospheric gas-particle partitioning of PAHs and for revealing the factors and mechanisms governing their geochemical cycling at air and water interfaces.

Keywords: PAHs; gas-particle partitioning; air-water exchange; Three Gorges Reservoir region (TGRR)

1. Introduction

Polycyclic aromatic hydrocarbons (PAHs), a group of ubiquitous persistent

organic pollutants (POPs), are aromatic organic compounds that composed of two or more fused benzene rings (Li et al., 2017). PAHs may be contained in crude and refined petroleum (i.e., petrogenic PAHs) and produced by combustion of fossil fuel and biomass burning (i.e., pyrogenic PAHs) (Ravindra et al., 2008; Zakaria et al., 2002). Due to their teratogenic, carcinogenic, and mutagenic effects, PAHs have become the important pollutants in environmental science research (Huang et al., 2017; Jiang et al., 2014).

On account of their semi-volatility, hydrophobicity and lipophilicity, PAHs have diverse and complicated environmental geochemical behaviors, such as atmospheric deposition, gas-particle partitioning, air-water/soil exchange and even absorption by plants (Fellet, et al., 2016; Wu et al., 2019). There have been studies concerning the gas-particle partitioning and air-water exchange of PAHs over the atmosphere of fresh waters. For example, Li et al. (2009) estimated air-water diffusion exchange flux of PAHs in a small urban lake in Guangzhou, China, based on a year-round monitoring. They revealed that the fluxes were predominantly controlled by the precipitation intensity in wet season whereas by atmospheric concentration in dry season. Verma et al. (2017) assessed the gas-particle partitioning of PAHs in a rural site close to Yamuna river, India, during post-monsoon and winter seasons. The regression parameters and the relationship between the partitioning coefficient and temperature suggested that the concentration of PAHs in the atmosphere is governed by local sources. Low molecular weight PAHs were found mainly in the gaseous phase and high molecular weight PAHs in the particulate phase. Recently, Tucca et al. (2020) estimated the air-water diffusive

exchange fluxes of PAHs in an oligotrophic North–Patagonian lake in Chile. They found that PAHs showed a net volatilization for lighter PAHs, and a net deposition trend for higher molecular weight PAHs. As regarding the occurrence of PAHs in atmosphere and water, these studies issued the multi-medium behavior of PAHs in regional perspective.

The Three Gorges Dam (TGD), one of the largest man-made hydropower projects in the world, has had a seasonal change in water level as a result of water storage in the winter (October-April) and release in summer (May-September) (Deng et al., 2016; Zhang et al., 2015). The water level rises to 175m during storage period, and decreases to 145m during discharge period, resulting in a unique water-level-fluctuation zone (WLFZ) along the Three Gorges Reservoir region (TGRR) (Jiang et al., 2018b; Yue et al., 2016). With a length of ~190 km and an area of ~350 km^2, environmental conditions of the WLFZ are influenced by intensive human activity (Ye et al., 2011; Huang et al., 2015). These studies showed that the formation of WLFZ changes the air-water interactions, and influences the transfer of contaminants from 'source to sink' in the TGRR.

The concentration of USEPA priority 16 PAHs in surface sediments of the WLFZ in TGRR was between 165 and 1653 ng/g, dominating as the main POPs in this region (Floehr et al., 2015). In the summer half year, the water level in the dam gradually decreases, exposing the WLFZ under the air and enabling the PAHs evaporate from water into atmosphere due to the relatively high temperature and more abundant light illumination and oxygen. In the winter half year, the water level gradually increases, re-

89 submerging the WLFZ under the water and enabling the PAHs trapped therein due to
90 surface runoff and interception effect from the TGD. This “trapped phenomenon” could
91 be enhanced by the relatively low temperature and anaerobic environment of WLFZ.
92 These two distinct water-air interactions could result in the different roles of the water
93 for the PAHs in the atmosphere over the WLFZ.

94 There have been studies focusing on the occurrence and transfer of PAHs in
95 water systems in TGRR, such as Deyerling et al. (2014), Wang et al. (2009) and Wolf
96 et al. (2013). Recently, we collected atmospheric samples from the WLFZ in winter and
97 summer, and found that 2-3 ring PAHs in summer was more likely to come from
98 volatilization from the water, while 5-6 ring PAHs in winter was mainly from biomass
99 combustion, revealing a seasonal "absorption-volatilization" conversion of PAHs in the
100 water (Wang et al., 2020). The water as a ‘source’ in summer and a ‘sink’ in winter for
101 PAHs thereby requires further study. To date, air-water exchange and gas-particle
102 partitioning of PAHs in atmosphere over the WLFZ at different water levels have not
103 received much attention.

104 The objectives of this study were to 1) unravel the mechanism of gas-particle
105 partitioning and air-water exchange of PAHs in different seasons; 2) to explore the
106 potential “volatilization from the water” and “deposition to the water” roles of PAHs
107 driven by water level manipulation under human disturbance. This study on the gas-
108 particle partition and air-water exchange of PAHs in WLFZ is therefore important for
109 understanding their different environmental geochemical behaviors during periods of
110 water storage (winter) and discharge (summer) in the TGRR.

2. Materials and methods

2.1 Sampling

Air and water samples were collected at Pengxi River wetland nature reserve, a typical part of WLFZ in TGRR (Figure 1). With an area of 41.07 km^2, the natural reserve is approximately 250 km upstream of the TGD, and has low residential density and almost no industrial activity. The water level of the reserve could increase to ~175 m in winter and drop to ~145 m in summer of the next year, making it an ideal site to conduct gas-particle partition and air-water exchange of PAHs in different seasons in WLFZ.

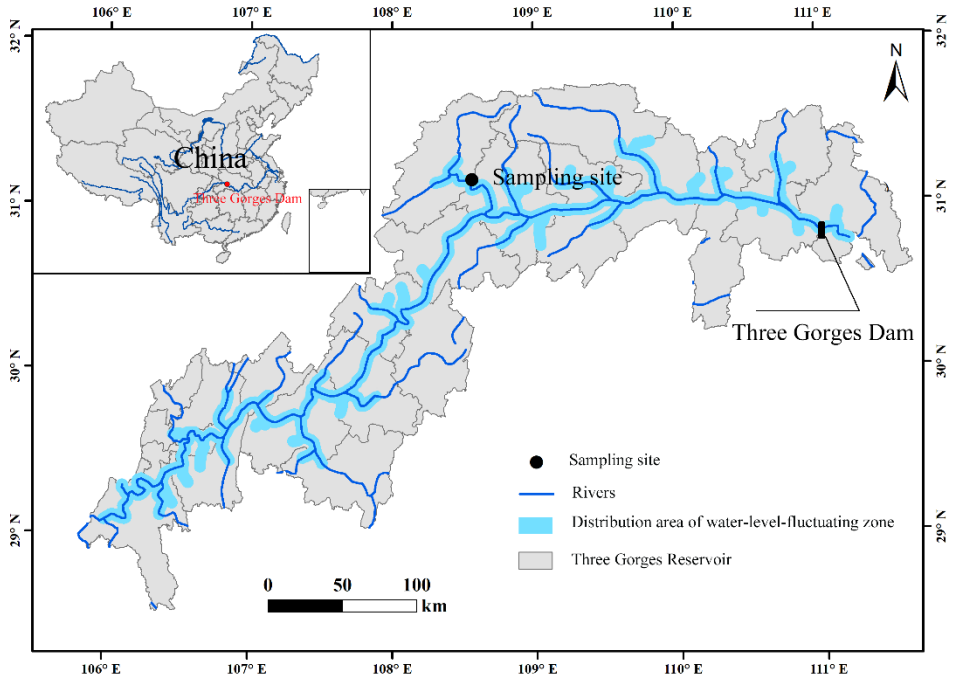

Figure 1 Sampling site at WLFZ of TGRR.

The sampling apparatus was placed on the roof of a three-story building, a super scientific monitoring station affiliated to Chongqing Forestry Bureau. This station has been used to observe the characteristics of carbonaceous pollutants in the atmosphere between different seasons associated with water levels in TGRR (Wang et al., 2020).

Air samples were collected via a high-volume air sampler (ASM-1, Guangzhou Mingye Huanbao Technology Company, Guangzhou, China) with a flow rate of approximately of 300 L/min. Total suspended particle (TSP) samples were collected on quartz fiber filters (20×25 cm^2, T2600, Pall Corporation, Port Washington, NY, USA) held in a metal frame and then polyurethane foam (PUF) plugs (6.5 cm in diameter, 7.5 cm in thickness, density 0.030 $g \cdot cm^{-3}$) were carried out using a glass holder to collect PAHs in the gas phase. Each sample was collected over 23.5-hours, from 9:00 a.m. to 8:30 a.m. of the following day. Two field blank samples were obtained for water-storage and water-release period respectively. Prior to sampling, the quartz fiber filters were wrapped in aluminum foil and baked in a muffle furnace for at least 4 h at 450 ℃. The PUF plugs were Soxhlet-extracted with dichloromethane (DCM) for 48 h. After drying, these PUF plugs were sealed in valve bags and stored in a desiccator. After sampling, all samples including the field blanks were stored at -20℃ until further analysis. There were both two parallel field blanks for the air and water samples. Surface water samples (10 L/sample) were collected using a lake water-rinsed/ river water-rinsed Teflon bucket adjoining the super scientific monitoring station. The water sampling site is ~100 m far away from the station. The samples were collected in the same location both in winter and summer. Using a vacuum pump, a pre-combusted glass fiber filter (GF/F, 50 mm in diameter, bore size 0.45 μm) was used to remove suspended solids. A glass column filled with Amberlite XAD-2 and XAD-4 resin (1:1 of total 30 g, Sigma-Aldrich, USA) was used for solid-phase extraction and enrichment of dissolved PAHs in the filtrate through a peristaltic pump. The XAD-2 and XAD-4 resin were pre-

cleaned using a Soxhlet extraction with dichloromethane (DCM) for 48 h. Finally, the solid-phase extraction column was wrapped with a parafilm and aluminum foil and stored at -20℃ as well. Twenty-two paired gas-particle (n=44) and water samples (n=44), from January 8 to January 17, 2019 (winter: high water level ~175m) and July 12 to July 23, 2019 (summer: low water level ~145m), were collected consecutively in this study. The sampling information and meteorological conditions are summarized in Table S1 in Supporting Information.

2.2 Sample analysis

Dichloromethane (DCM) was used to Soxhlet extract PAHs from the quartz fiber filters and PUF plugs after adding a known PAHs standard sample. The standard sample consisted of deuterated naphthalene (Nap-d_8, m/z 136), deuterated acenaphthene (Ace-d_{10}, m/z 164), deuterated phenanthrene (Phe-d_{10}, m/z 188), deuterated chrysene (Chr-d_{12}, m/z 240) and deuterated perylene (Per-d_{12}, m/z 264). After 48h, the DCM was rotary evaporated to about 5 mL at 30℃ and 40 rpm/min in a vacuum rotary evaporator and solvent-exchanged to hexane (HEX). The concentrates were evaporated to about 2 mL by N_2 with a purity of 99%. The chromatography columns (8 mm in diameter, 20 cm in length, 3 cm deactivated Al_2O_3, 3 cm SiO_2 and 1 cm Na_2SO_4 from the bottom to top) were used for clean-up and fractionation. Subsequently, the columns were rinsed three times with 15 mL DCM/HEX (1:1, v:v) and concentrated again with N_2 to a volume of 500 μL. For water samples, DCM/HEX (1:1, v:v) was used to rinse the solid-phase extraction columns and then treated in the same way as the air samples described above. An Agilent GC 6890 N equipped with DB5-MS column (30 m×0.25 mm×0.25

μm) coupled with Agilent 5975C MSD was used for PAHs determination. GC-MS operation was programmed as follows: initial temperature of 60℃ for 2 min, ramped to 290℃ at 3 ℃/min and held for 20 min and injected with the split-less mode. The post-run time was 5 min at 310 ℃. Hexamethylbenzene (HMB) was added as an internal standard for GC-MS analysis.

The targeted PAHs were USEPA 16 priority PAHs. The following are the number of rings, names and abbreviation of them: 2-3 ring (6 species): naphthalene (Nap); acenaphthylene (Ac), acenaphthene (Ace), fluorene (Fl), phenanthrene (Phe), anthracene (Ant); 4-ring (4 species): fluoranthene (Flu), pyrene (Pyr), benzo[a]anthracene (BaA), chrysene (Chr); 5-6 ring (4 species): benzo[b]fluoranthene (BbF), benzo[k]fluoranthene (BkF), benzo[a]pyrene (BaP), dibenzo[a,h]anthracene (DBA); indeno[1,2,3-cd]pyrene (IP), benzo[ghi]perylene (BghiP).

2.3 Quality assurance/ Quality control (QA/QC)

The purity of the organic solvent (DCM and HEX) was 95% HPLC grade in this study. Prior to sample processing, all the glass apparatuses were washed and dipped in hot potassium dichromate and sulfuric acid mixed solution. Apparatus was subsequently rinsed with de-ionized water (18.2 MΩ Milli-Q) successively then wrapped in aluminum foil and heated for at least 4 hours at 450℃ in a muffle furnace. All apparatuses were rinsed three times with DCM or HEX before use. Surrogate recoveries in the gas phase samples were 61%±10% for Nap-d_8, 70%±5% for Ace-d_{10}, 90%±4% for Phe-d_{10}, 98%±4% for Chr-d_{12} and 103%±5% for Per-d_{12}, respectively. For the TSP samples, they were 62.3%±8% for Nap-d_8, 82.7%±5% for Ace-d_{10}, 92.5%±5%

for Phe-d_{10}, 101.8%±7% for Chr-d_{12} and 111.5%±10% for Per-d_{12}, respectively. For the dissolved phase in water samples, they were 59.3%±9% for Nap-d_8, 66.7%±9% for Ace-d_{10}, 80.3%±10% for Phe-d_{10}, 87.9%±11% for Chr-d_{12} and 100.2%±10% for Per-d_{12}, respectively. The method detection limits (MDLs) were the average field blank plus three times the standard deviation and were 0.019-0.35 pg/m^3 for the air samples and 0.15-1.92 pg/L for the water samples (Wu et al., 2017). Aside from Nap, the other species of PAHs were almost under detection method for the field blanks and other blank samples. The sample results were displayed as blank corrected values by subtracting the average blank concentrations from each sample.

2.4 Gas-particle partitioning

The partitioning behavior of PAHs between gas and particle phase can be described by gas-particle partition coefficient (K_p, $m^3 \cdot \mu g^{-1}$) (Jenkins et al., 1996; Sitaras et al., 2004) as follows:

$$K_p = \frac{C_p}{C_g \times TSP} \quad (1)$$

Where C_p and C_g are PAHs concentrations ($ng \cdot m^{-3}$) in the particle and gas phase, respectively; TSP is the total suspended particle concentration ($\mu g \cdot m^{-3}$).

The distribution of PAHs in the atmosphere can be divided into adsorption and absorption (Simcik et al., 1998; Terzi and Samara, 2004). After introducing the vapor pressure of the subcooled liquid (P_L^0), the linear relationship of $\log K_p$ and $\log P_L^0$ was developed to characterize both mechanisms of organic matter absorption and particle surface adsorption (Simcik et al., 1999), with the equation:

$$\log K_p = m_r \log P_L^0 + b_r \quad (2)$$

Where the slope value (m_r) could indicate equilibrium state and dominant mechanism of distribution, and the intercept value (b_r) is related to the properties of aerosol particles. The temperature-dependent P_L^0 of PAHs was calculated as:

$$\log P_L^0 = \frac{m_L}{T} + b_L \quad (3)$$

Where T is the average temperature during the sampling time. The m_L and b_L values for PAHs species are shown in Table S2 (Odabasi et al., 2006). Theoretically, the gas-particle distribution process is in equilibrium with a slope value of -1 (Pankow, 1994). If $m_r < -1$, the adsorption onto the particle surface is dominant; If $m_r > -0.6$, the distribution is mainly affected by the absorption into the organic matter of particles; And if $-1 < m_r < -0.6$, adsorption and absorption jointly affect the distribution (Goss and Schwarzenbach, 1998). In equilibrium, the $\log K_p$-$\log P_L^0$ model can be simplified as Zhang et al. (2018):

$$\log K_p = -\log P_L^0 + \log f_{OM} - 5.22 \quad (4)$$

Where f_{OM} is the mass fraction of organic matter (OM), and could be calculated as OM=1.6OC (Chan et al., 2010).

As octanol is the solvent usually used as the reference for OM in studies, the distribution of PAHs between gas and OM (K_{OM}) can be empirically viewed as its octanol-air distribution coefficient (K_{OA}) (Harner and Bidleman, 1998; Lohmann et al., 2000). The linearly dependent model of $\log K_p$ and $\log K_{OA}$ can then be expressed as Finizio et al. (1997):

$$\log K_p = m \log K_{OA} + b \quad (5)$$

Where the temperature-dependent K_{OA} values can be obtained by:

$$\log K_{OA} = B/T + A \quad (6)$$

The A and B values for targeted PAHs are shown in Table S1. Ideally, the m value should be near ±1 under the equilibrium condition. The equations for the absorption and the adsorption models are summarized in Supporting Information.

2.5 Air-water exchange

The exchange between dissolved and gas phase PAHs was quantitatively estimated by the widely applied Whitman two-film resistance model (Schwarzenbach et al., 2003). The flux of PAHs across the air-water interface is given by Wania et al. (1998):

$$F = Kol \cdot (C_w - C_a / H') \quad (7)$$

Where C_w (ng/m^3) and C_a (ng/m^3) are the concentrations of PAHs in the water and the atmosphere, respectively. H' is the dimensionless Henry's law constant. Kol (m/d) is the overall mass transfer coefficient (Wang et al., 2013), which is defined as:

$$\frac{1}{Kol} = \frac{1}{K_w} + \frac{1}{K_a H'} \quad (8)$$

Where K_w and K_a are the mass transfer rates through the water and air layer film, respectively (Wu et al., 2017). K_w can be expressed as Liu et al. (2016):

$$K_w = 0.65 \times 10^{-3} \times \left(S_{CW,PAHs}/S_{CW,CO2}\right)^{-0.67},\ U_{10} \leqslant 4.2 m/s \quad (9)$$

$$K_w = (0.79\ U_{10} - 0.68) \times 10^{-3} \times \left(\frac{S_{CW,PAHs}}{S_{CW,CO2}}\right)^{-0.5},\ U_{10} > 4.2 m/s \quad (10)$$

K_a can be expressed as McDonough et al. (2016):

$$K_a = (0.2\ U_{10} + 0.3) \times \left(D_{PAHs,a}/D_{H2O,a}\right)^{0.67} \quad (11)$$

Where U_{10} (m/s) is the wind velocity at a reference height of 10 m, $S_{CW,PAHs}$ and $S_{CW,PAHs}$ are the dimensionless Schmidt number of PAHs and CO_2, $D_{W,PAHs}$ (cm^2/s) and

258 $D_{W,CO2}$ (cm^2/s) are the molecular diffusivities of PAHs and CO_2 in the water,
259 respectively. The other equations for calculating the relevant parameters in K_w and K_a
260 are also summarized in Supporting Information.

261 **2.6 Uncertainty for exchange flux estimation**

262 The uncertainty of the estimated flux was calculated by the error propagation
263 analysis method derived from Shoemaker et al. (1974), which has been widely used by
264 Feng et al. (2021b) and Liu et al. (2016). The error caused by random uncertainty was
265 calculated as:

266 $$\sigma^2(F)=\left(\frac{\partial F}{\partial K_{ol}}\right)^2(\sigma K_{ol})^2+\left(\frac{\partial F}{\partial C_W}\right)^2(\sigma C_W)^2+\left(\frac{\partial F}{\partial C_a}\right)^2(\sigma C_a)^2 \quad (12)$$

267 Based on the measured samples and recoveries, the error coefficients of C_w and C_a
268 were estimated to be 20% and the error value of K_{ol} was assumed to be 40% to cover
269 the uncertainties in the air-water mass transfer coefficients and wind speed (Bamford et
270 al., 1999; Nelson et al., 1998).

271 The overall propagated error associated with the calculated of the PAH air-water
272 exchange fluxes ranged between 2% and 1069%, with an average 95%. Our result was
273 higher than that reported by Fang et al. (2008) (51%), but were close to those reported
274 by Cheng et al. (2013) (102%) and Feng et al. (2021b) (110%). Most of the errors
275 associated with the fluxes were attributed to the K_{ol} because it was the only value that
276 was not measured directly (Bamford et al., 1999; Nelson et al., 1998).

277 **3 Results and discussion**

278 **3.1 Occurrence of PAHs**

279 The sum of USEPA priority 16 PAHs (thereafter as 16 PAHs), in both the

atmosphere (gas and particle phase) and water samples are shown in Table 1. The concentrations of the individual PAHs are in Table S3. IP, DBA, BghiP were below detection limit in all gas phase samples. The concentrations of the 16 PAHs in the particle phase averaged at 66.63±9.15 ng/m^3 in winter and 8.43±2.95 ng/m^3 in summer, respectively. For the gas phase, they were 28.47±4.79 ng/m^3 in winter and 10.57±1.51 ng/m^3 in summer, respectively. Particulate PAHs dominated in winter, accounting for 70.1% of the total. In summer, gaseous PAHs dominated, contributing 54.7% of the total. In the water, the concentrations of dissolved PAHs of WLFZ averaged at 38.65±6.37 ng/L in winter while in summer the average was 56.53±8.86 ng/ L.

Table 2 shows the mean concentrations of the 16 PAHs in the atmosphere (gas and aerosol phases) and water (dissolved phase) of the WLFZ at TGRR compared with other studies worldwide. The mean value of PAHs in aerosol and gas phase at TGRR was lower than and Lake Taihu in China by a factor of 2 - 5 (Tao et al., 2017), and comparable with Pearl River Estuary, China (Lao et al., 2021). They were much higher than Marginal seas of Arctic Ocean (Na et al., 2021), Coral Reef Area of South China Sea (Feng et al., 2021b; Zhang et al., 2021a). For dissolved PAHs in water, the concentrations in TGRR were lower than Yangtze River Estuary, East China Sea (Jiang et al., 2018a), but higher than in the Coastal region of Incheon, South Korea (Kim and Chae, 2016) and Panguipulli Lake, Chile (Tucca et al., 2020).

Table 1. Summary of 16 PAHs in atmosphere (gas and particle phase) and water samples collected from Pengxi River Wetland Nature Reserve. (nd- not detected)

Compound	Particle phase (ng/m^3)	Gas phase (ng/m^3)	Air samples (ng/m^3)	Water samples (ng/L)

	Mean	SD	Mean	SD	Mean	SD	Mean	SD
(a)After submergence, winter (2019, 01)								
Nap	2.35	0.12	2.09	0.63	4.44	0.65	19.80	5.14
Ac	0.16	0.03	0.91	0.44	1.07	0.44	2.66	1.01
Ace	0.02	0.01	1.47	0.26	1.49	0.26	2.10	1.44
Fl	0.28	0.09	3.71	0.69	3.99	0.68	5.72	0.96
Phe	2.80	0.79	14.04	2.30	16.84	2.18	7.87	3.32
Ant	0.35	0.05	0.66	0.21	1.01	0.25	0.84	0.27
Flu	5.67	1.09	3.14	0.52	8.82	1.29	0.87	0.44
Pyr	5.35	0.77	1.94	0.37	7.28	1.03	0.90	0.27
BaA	3.16	0.51	0.13	0.05	3.30	0.55	nd	nd
Chr	5.14	0.63	0.32	0.06	5.46	0.64	nd	nd
BbF	13.79	2.01	0.02	0.01	13.81	2.01	nd	nd
BkF	3.37	0.57	0.03	0.01	3.40	0.57	nd	nd
BaP	5.78	1.44	0.03	0.01	5.81	1.45	nd	nd
DBA	1.26	0.21	nd	nd	1.26	0.21	nd	nd
IP	9.90	1.84	nd	nd	9.90	1.84	nd	nd
BghiP	7.22	1.40	nd	nd	7.22	1.40	nd	nd
∑PAHs	66.63	9.15	28.47	4.79	95.10	13.03	38.65	6.37
(b)Before submergence, summer (2019, 07)								
Nap	2.36	0.09	0.89	0.13	3.25	0.19	25.28	5.42
Ac	0.02	0.01	0.16	0.06	0.17	0.06	0.96	0.25
Ace	0.01	0.01	0.05	0.02	0.05	0.02	3.63	1.10
Fl	0.05	0.02	0.49	0.12	0.55	0.14	13.04	5.64
Phe	0.22	0.08	4.63	0.76	4.85	0.84	11.47	2.29
Ant	0.07	0.02	0.19	0.04	0.25	0.05	1.00	0.23
Flu	0.28	0.14	1.94	0.26	2.21	0.38	0.63	0.17
Pyr	0.37	0.21	1.15	0.20	1.52	0.37	0.5203	0.14
BaA	0.28	0.14	0.08	0.02	0.35	0.16	0.02	0.05
Chr	0.40	0.20	0.40	0.11	0.81	0.27	0.02	0.04
BbF	0.99	0.51	0.12	0.03	1.11	0.53	0.15	0.47
BkF	0.32	0.15	0.02	0.004	0.34	0.15	0.04	0.13
BaP	0.66	0.36	0.06	0.01	0.71	0.38	0.01	0.03
DBA	0.14	0.06	nd	nd	0.14	0.06	0.001	0.004
IP	1.28	0.65	nd	nd	1.28	0.65	0.004	0.01
BghiP	1.00	0.51	nd	nd	1.00	0.51	0.004	0.01
∑PAHs	8.43	2.95	10.17	1.51	18.60	4.34	56.53	8.86

Table 2. Comparisons of the mean concentrations of 16 PAHs in atmosphere (gas and aerosol phases) and water (dissolved phase) of WLFZ at TGRR with other places.

Sampling site	Sampling period	Aerosol phase (ng/m^3)	Gas phase (ng/m^3)	Dissolved phase (ng/L)	References
WLFZ in TGRR, China	2019.01.08-2019.01.17	66.62	28.47	40.74	This study
WLFZ in TGRR, China	2019.07.12-2019.07.23	8.42	10.17	56.78	This study
Pearl River Estuary, China	2019.08.18-2019.08.25	1.14	184.67	35.65	Lao et al., 2021
Marginal seas of Arctic Ocean	2018.07-2018.09	0.05	1.66	133.90	Na et al., 2021
Coral Reef Area of South China Sea	2018.03.21-2018.04.12	0.83	41.25	7.94	Feng et al., 2021b
Coral Reef Regions South China Sea	2015.05.20-2015.07.04	0.15	6.74	252.28	Zhang et al., 2021a
Panguipulli Lake, Chile	2017.03-2017.08	—	11.62	0.96	Tucca et al., 2020
Yangtze River Estuary, East China Sea	2014.03.27-2015.01.18	3.4	4.4	61.4	Jiang et al., 2018a
Taihu Lake, China	2015.03.30-2016.01.28	90.77	106.57	294.20	Tao et al., 2017
Coastal region of Incheon, South Korea	2013.10-2014.12	—	37.0	9.34	Kim and Chae, 2016

3.2 Gas-particle partitioning of PAHs

The lgK_p values of 13 PAHs (3 species were under detection limit in water sample) in the atmosphere of WLFZ in the TGRR in winter (high water level) and summer (low water level) are summarized in Table S4. Figure 2 compares the measured and predicted lgK_p of PAHs using the dual octanol-air/soot-air model. The average lgK_p of 2-5 ring PAHs were -1.86 ± 0.28, -2.86 ± 0.68, -1.09 ± 0.56 and 0.53 ± 0.44 in winter, respectively. In summer, they were -1.06 ± 0.14, -2.43 ± 0.37, -1.71 ± 0.58 and -0.46 ± 0.21, respectively. As shown in Figure 2, the K_p displays an increasing trend with the molecular weight of PAHs, which is similar to other studies (Hu et al., 2019). Low ring PAHs have higher vapor pressures and Henry's coefficients, making them readily distribute in the gas phase. However, high ring PAHs have relatively low volatility and tend to combine with particles (Barrado et al., 2012). The K_p of high ring PAHs in summer were lower than those in winter, which could be related to meteorological conditions as solar radiation and high ambient temperature in summer are conducive to the volatilization of PAHs from the particle to the gas phase, resulting in the decrease of K_p (Jia et al., 2021). In winter, high relative humidity lead to high aerosol liquid water content, promoting the adsorption of aerosols by PAHs and increasing the K_p value (Hu et al., 2019). Non-exchangeable compositions of PAHs are fixed in aerosols generated by combustion from fossil fuels and biomass, making them difficult to migrate into the gas phase. This could be an important reason why K_p values of some low ring PAHs, such as Nap, Ace and Fl, were still high (Harner and Bidleman, 1998).

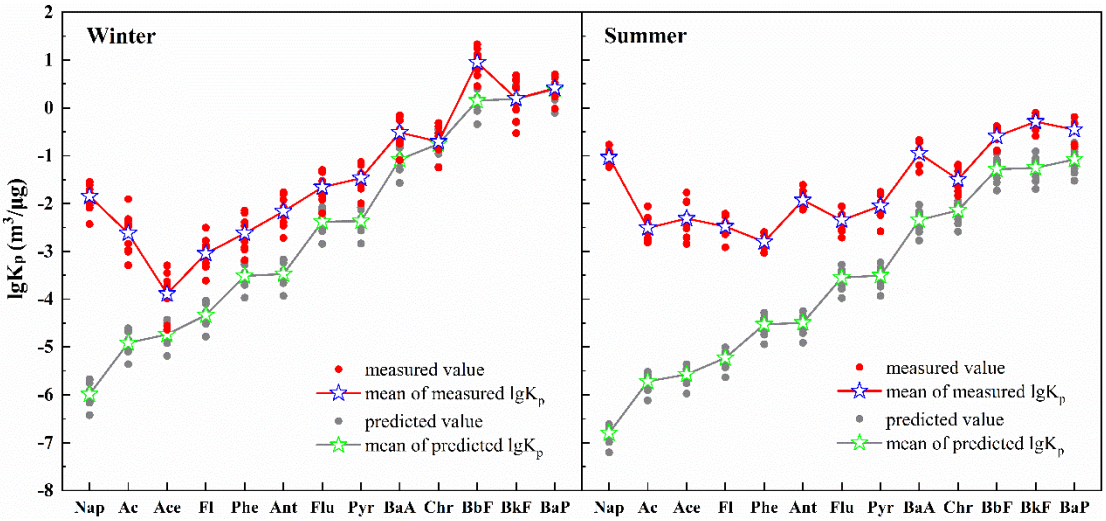

Figure 2 The measured and predicted lgK$_p$ of PAHs using the dual octanol-air/soot-air model.

The regression results of lgK$_p$-lgP$_L^0$ and lgK$_p$-lgK$_{OA}$ for atmospheric PAHs of TGR are shown in Figure 3. The slope of lgK$_p$-lgP$_L^0$ in winter and summer was -0.53 and -0.27, respectively. For the interception, they were -3.05 and -2.13, respectively. The results showed that the distribution of gas-particle partition were mainly influenced by the absorption into particulate organic matter (Goss and Schwarzenbach, 1998). The slopes of lgK$_p$-lgK$_{OA}$ in winter and summer was 0.50 and 0.27, respectively. For the interception, they were -6.19 and -3.92, respectively. These results both indicated the disequilibrium of PAHs distribution in the atmosphere of WLFZ in TGRR (Zhang et al., 2018). Indeed, factors including pollution source input, temperature variation, humidity and particle properties (such as adsorption point and organic matter activity coefficient) as well as irreversible adsorption of organic matter in particles would all affect the gas-particle distribution (Goss and Schwarzenbach, 1998; Simcik et al., 1998). PAHs emitted to the atmosphere would gradually reach an equilibrium state after a process of atmospheric deposition, gas-particle reaction and chemical transformation

(Lohmann et al., 2000; Simcik et al., 1998). According to Akyüz and Çabuk, (2010), slopes of lgK_p-lgP_L^0 close to −1 indicate that the PAHs transport from over long distances to sampling site, whereas the slopes far from −1 denote the contribution of local sources. The slope observed in this study was rather far from −1. This indicated that the PAHs were mostly from location sources. The adsorption–desorption equilibrium between the gas and particle phases has not been established. Back trajectory analysis at 100 m (red),700 m (green) and 2000 m (blue) of the individual 72-hour arriving at sampling site during the sampling period are shown in Figure S1. The parcels in the two seasons from nearby of East Chongqing were both mainly observed at 100 m. The air parcels in summer were faster than those in winter, making the transport paths relatively short. Considering the mountainous location of the sampling site, it is reasonable to conclude that a short transport pathway from local Chongqing had an effect on the gas-particle partitioning of PAHs.

The slope of lgK_p-lgP_L^0 and lgK_p-lgK_{OA} in summer was shallower than those in winter. One possible reason could be the effect from ambient temperature, since the higher temperature in summer would prompt more organic compounds with higher vapor pressures to evaporate into the atmosphere. These compounds could then be absorbed by particles, resulting in a deviation between slope and equilibrium value. In this study, temperatures in summer and winter were 25.5-34 °C and 5-7 °C, with a mean of 29.8 °C and 6.1 °C, respectively. Another possible reason could be ascribed to the sorptive properties of the atmospheric particles from different sources between summer and winter (Hu et al., 2019). Fossil fuel and biomass combustion were the important

sources of PAHs in the atmosphere around the reservoir area (Hu et al., 2019; Feng et al., 2021a). Incomplete combustion of these fuels is conducive to the formation of non-exchangeable components, as are forest fires and volatilization of diesel/ petroleum residues in summer.

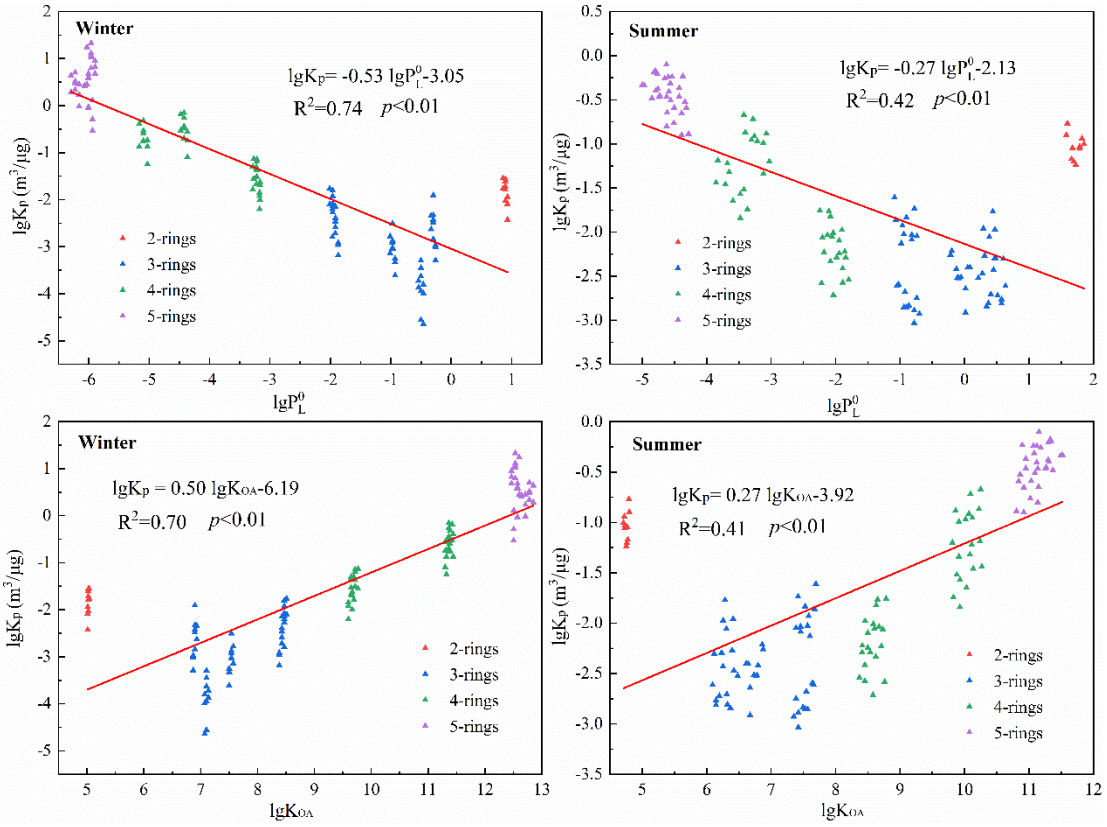

Figure 3 The regression results of lgK_p-lgP_L^0 and lgK_p-lgK_{OA} for atmospheric PAHs of TGR.

Table 3 summarize a comparison of Φ_{meas}/Φ_{pred} for atmospheric PAHs from the equilibrium states of lgK_p-lgP_L^0 and lgK_p-lgK_{OA} models, and the dual octanol-air/soot-air model. Φ=Cp/(Cp+Cg), where Cp and Cg are PAHs concentrations (ng/m^3) in the particle phase and gas phase, respectively. The results showed using the dual model the predicted values of Φ were closer to the measured values from field sampling, indicating that organic matter and elemental carbon were important factors affecting

the partitioning (Figure 3). The elemental carbon in aerosols has a strong adsorption effect on PAHs, and therefore the elemental carbon-air distribution coefficient (K_{SA}) could be a vital parameter for prediction (Dachs and Eisenreich, 2000). The predicted Φ for low ring PAHs (2-3 rings) varied greatly among the three models; while for high ring PAHs (4-5 rings), they were good agreement with the measured value. Therefore, the equilibrium state prediction model was more suitable for the gas-particle partitioning of 4-5 ring PAHs. For the dual model (Figure 3), the predicted lgK_p underestimated the actual gas-particle partitioning determind from the field sampling, and the deviation decreased with the ring number of PAHs. The lgK_p of 2-5 ring PAHs in winter were underestimated by 4.14 ± 0.14, 1.33 ± 0.57, 0.56 ± 0.33 and 0.28 ± 0.42 units, respectively. In summer, they were underestimated by 5.77 ± 0.22, 2.68 ± 0.60, 1.17 ± 0.36 and 0.76 ± 0.19 units, respectively. Low ring PAHs have strong diffusivity, and readily reach an equilibrium state, but this state was vulnerable during the field sampling process. For example, PAHs with high volatility originated from incomplete combustion were wrapped by particles and therefore could not interact between different phases (Simcik et al., 1998). The deviation between Φ_{meas} and Φ_{pred} in winter was less than in the summer. Hence, the more active migration, diffusion and chemical reactions of PAHs in summer could affect the prediction bias of these models.

Table 3. Comparison of Φ_{meas}/Φ_{pred} for atmospheric PAHs from the equilibrium states of lgK_p-lgP_L^0 and lgK_p-lgK_{OA} models, and the dual octanol-air/soot-air model.

PAHs	2019/01 (high water level period)			2019/07 (low water level period)		
	lgK_p-lgP_L^0	lgK_p-lgK_{OA}	Dual Model	lgK_p-lgP_L^0	lgK_p-lgK_{OA}	Dual Model
Nap	4.75×10^4	2.79×10^5	6.39×10^3	1.38×10^6	2.26×10^6	1.73×10^5
Ac	9.98×10^2	1.22×10^3	1.81×10^2	1.00×10^4	9.58×10^3	1.65×10^3

Ace	47.06	57.63	8.82	9.27×10^3	8.75×10^3	1.61×10^3
Fl	85.86	1.14×10^2	18.87	2.74×10^3	2.80×10^3	5.50×10^2
Phe	23.16	35.06	6.87	2.05×10^2	2.34×10^2	52.37
Ant	44.84	68.41	13.52	1.11×10^3	1.27×10^3	2.89×10^2
Flu	4.96	8.71	2.52	41.36	56.54	14.97
Pyr	5.79	8.59	2.83	66.93	92.24	24.28
BaA	1.37	1.19	1.10	16.84	13.19	6.86
Chr	1.03	1.16	1.01	4.65	7.90	2.86
BbF	1.01	1.01	1.01	1.86	2.29	1.51
BkF	1.00	1.01	1.00	1.91	2.35	1.57
BaP	1.00	1.00	1.00	1.50	1.79	1.31

3.3 Air-water exchange

Using the associated equations shown above, we calculated the air-water exchange fluxes of PAHs in winter and summer. The air-water exchange fluxes of 12 individual PAHs (Nap, DBA, IP and BghiP not included) in winter (high water level period) and summer (low water level period) are summarized in Table S5. Figure 4 shows the variation of exchange fluxes of 12 PAHs based on the collected samples. The flux ranged from -0.36 ng/m^2/d (Fla at 2019/01) to 3.19 ng/m^2/d (Flu at 2019/07). The negative values represent net deposition from air to water, while positive values represent the volatilization of PAHs from water into air. Among them, 3-ring PAHs showed a trend of net volatilization. Flu had the highest flux, accounting for 43.1% and 49.5% of the total in winter and summer, respectively. The next highest flues were from Ace (22.6% and 17.7%) and Phe (4.1% and 25.9%). 4-ring PAHs favored deposition from the air into the water. The deposition fluxes of 5-ring PAHs were rather low owning to their low concentrations in the water phase. As regards the total exchange of PAHs, the flux in TGR was lower than the Northwest Pacific Ocean (15PAHs, -54 to 107 ng/m^2/d) (Wu et al., 2017) but comparative with the coral reef region in South China Sea (15PAHs, -55.9 to -0.86 ng/m^2/d) (Zhang et al., 2021a).

The direction and flux of PAHs exchange at the air-water interface are related to their physical and chemical properties, such as molecular weight, vapor pressure, as well as environmental factors such as temperature and wind speed (Chen et al., 2016; Wu et al., 2017; Wu et al., 2019). Three-ring PAHs are relatively water-soluble and could be abundant in the water phase (Zhang et al., 2021b). Due to their high vapor pressure and Henry's constant, they generally show a trend of volatilization from the water into the gas phase. By contrast, 4-5 ring PAHs readily occur in the particle phase (Zhang et al., 2021a) and deposit into water via atmospheric deposition. In this study, 3-ring PAHs were tended to volatilize from water into the gas phase, 4-5 ring PAHs were favored to deposit from the air into the water. This was confirmed by the results of our study and consistent with reported results from the Bohai and Yellow Seas (Chen et al., 2016) and the northwestern Pacific Ocean (Wu et al., 2017).

The seasonal variation of PAHs air-water exchange flux mainly related to ambient temperature (Ruge et al., 2015; Wu et al., 2019). In this study, the average surface water temperature was 10.4 ℃ in winter and 28.4 ℃ in summer. LMW PAHs have low evaporation enthalpy, and their water-gas exchange process is significantly affected by the temperature (McDonough et al., 2014). High temperature promotes the volatilization of PAHs from water into gas phase, and weakens the absorption of PAHs by the water (Zhang et al., 2021a). Therefore, the air-water exchange flux of LMW PAHs in summer is generally higher than those in winter. In addition, meteorological factors such as wind speed and wind direction could affect air-water exchange. For example, Wu et al. (2017) found that higher wind speed promoted the volatilization of

3-ring PAHs from water into air while Zhang et al. (2021a) showed that the air masses originating from different directions had effect on the PAHs air-water exchange flux.

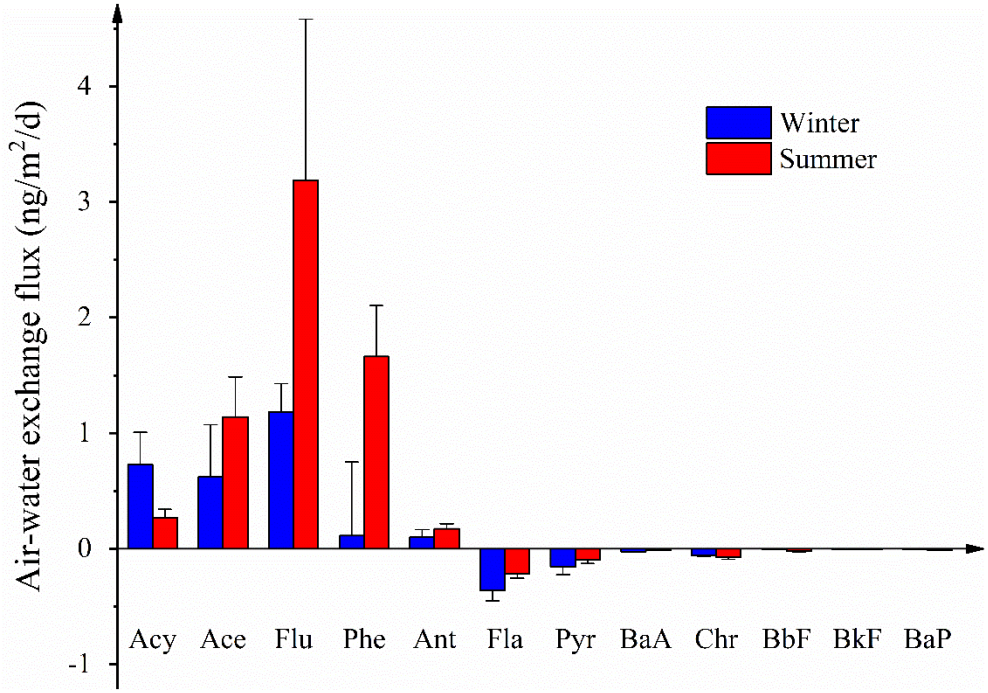

Figure 4 The seasonal variation of exchange fluxes of 12 PAHs based on the collected samples.

Although this study was limited to two seasonal datasets collected from only one location, information of the air-water exchange of PAHs in WLFZ of TGRR could still be obtained. Apart from air-water exchange, there were two other ways that PAHs could interact with the surface water, via atmospherically dry and wet deposition. Larger scale studies based on multiple sites and four seasonal samples are needed to reveal higher resolution temporal-spatial variations of air-water exchange of PAHs. Further study on the atmospheric wet and dry deposition of PAHs to identify the role of water as a "source" or "sink" in WLFZ should be considered, and would prove to be interesting and fruitful. Moreover, PAHs concentrations will be measured in different depth of the water column, providing a good chance to assess the effect of vertical transport on the

452 air-water exchange at the reservoir.

453 **4 Conclusions**

454 This study provides the first data sets of gas-particle partitioning and air-water
455 exchange of PAHs in WLFZ in TGRR of China. The concentrations of USEPA 16PAHs
456 in the water and air averaged 47.6 ± 7.62 ng/L and 56.9 ± 8.69 ng/m^3, respectively. The
457 seasonal average of PAHs in the air in winter were higher than those in summer; while
458 the opposite was true for PAHs in the water. The regression results of lgK_p-lgP_L^0 and
459 lgK_p-lgK_{OA} complemented well each other, both indicating the non-equilibrium
460 distribution of PAHs in the atmosphere of WLFZ in TGRR. The slope of lgK_p-lgP_L^0
461 and lgK_p-lgK_{OA} in summer was shallower than those in winter. The Φ_{pred} were closer
462 to the Φ_{meas} from field sampling, indicating the important influence of organic matter
463 and elemental carbon affecting partitioning. The deviation between Φ_{meas} and Φ_{pred} in
464 winter was less than that in summer. Three-ring PAHs showed a trend of net
465 volatilization from water in air while 4~5-ring PAHs favored deposition from the air
466 into the water. Under these conditions, there should be more concern regarding the
467 atmospheric wet and dry deposition of PAHs as identifying the role of "source" or "sink"
468 PAHs in the water of WLFZ in TGRR.

469 **Acknowledgement**

470 This work was supported by the National Natural Science Foundation of China
471 (NSFC) (No: 42077319, 41603102), National Key R&D Program of China (No:
472 2019YFC1805500); Technological Innovation and Application Development Key
473 Projects of Chongqing Municipality, China (No: CSTB2022TIAD-KPX0202,

cstc2019jscx-gksbX0060).

References

Akyüz, M., Çabuk, H., 2010. Gas-particle partitioning and seasonal variation of polycyclic aromatic hydrocarbons in the atmosphere of Zonguldak, Turkey. Sci. Total Environ. 408, 5550-5558.

Bamford, H. A., Poster, D. L., Baker, J. E., 1999. Temperature dependence of Henry's law constants of thirteen polycyclic aromatic hydrocarbons between 4°C and 31°C. Environ. Toxicol. Chem. 18, 1905-1912.

Barrado, A.I., Garcia, S., Barrado, E., Perez, R.M., 2012. PM2.5-bound PAHs and hydroxy-PAHs in atmospheric aerosol samples: Correlations with season and with physical and chemical factors. Atmos. Environ. 49, 224-232.

Chan, T.W., Huang, L.， Leaitch, W.R.， Leaitch, W.R., Sharma, S., Brook, J.R., Slowik, J.G., Abbatt, J.P.D., Brickell, P.C., Liggio, J., Li, S.M., Moosmuller, H., 2010, Observations of OM/OC and specific attenuation coefficients (SAC) in ambient fine PM at a rural site in Central Ontario, Canada． Atmos. Chem. Phys. 10(5): 2393-2411．

Cheng, J.O., Ko, F.C., Lee, C.L., Fang, M.D., 2013. Air-water exchange fluxes of polycyclic aromatic hydrocarbons in the tropical coast, Taiwan. Chemosphere. 90, 2614-2622.

Chen, Y.J., Lin, T., Tang, J.H., Xie, Z.Y., Tian, C.G., Li, J., Zhang, G., 2016. Exchange of polycyclic aromatic hydrocarbons across the air-water interface in the Bohai and Yellow Seas. Atmos. Environ. 141, 153-160.

496 Dachs, J., Eisenreich, S.J., 2000. Adsorption onto aerosol soot carbon dominates gas-
497 particle partitioning of polycyclic aromatic hydrocarbons. Environ. Sci. Technol
498 34, 3690-3697.
499 Deng, K., Yang, S.Y., Lian, Y.G., Li, C., Yang, C.F., Wei, H.L., 2016. Three Gorges
500 Dam alters the Changjiang (Yangtze) river water cycle in the dry seasons:
501 Evidence from H-O isotopes. Sci. Total Environ. 562, 89-97.
502 Deyerling, D., Wang, J.X., Hu, W., Westrich, B., Peng, C.R., Bi, Y.H., Henkelmann, B.,
503 Schramm, K-W., 2014. PAH distribution and mass fluxes in the Three Gorges
504 Reservoir after impoundment of the Three Gorges Dam. Sci. Total Environ. 491,
505 123-130.
506 Fang, M.D., Ko, F.C., Baker, J.E., Lee, C.L., 2008. Seasonality of diffusive exchange
507 of polychlorinated biphenyls and hexachlorobenzene across the air-sea interface
508 of Kaohsiung Harbor, Taiwan. Sci. Total Environ. 407, 548-565.
509 Fellet, G.; Posic, F.; Licen, S.; Marchiol, L.; Musetti, R.; Tolloi, A.; Barbieri, P.; Zerbi,
510 G., 2016. PAHs accumulation on leaves of six evergreen urban shrubs: A field
511 experiment. Atmos. Pollut. Res. 7, 915-924.
512 Feng, T., Wang, F.W., Yang, F.M., Li, Z.L., Lu, P.L., Guo, Z.G., 2021a. Carbonaceous
513 aerosols in urban Chongqing, China: Seasonal variation, source apportionment,
514 and long-range transport. Chemosphere 285, 131462.
515 Feng, Z.Y., Wang, C.L., Zhang, C.C., Wang, W.Z., Wang, J.J., Li, Y.L., Zou, X.Q.,
516 2021b. Air-Water Exchange and Gas-Particle Partitioning of Polycyclic Aromatic
517 Hydrocarbons (PAHs) in Coral Reef Areas of the South China Sea. J. Geophys.

518 Res-Atmos. 126, 9: e2020JD033399.
519 Floehr, T., Scholz-Starke, B., Xiao, H.X., Koch, J., Wu, L.L., Hou, J.L., Wolf, A.,
520 Bergmann, A., Bluhm, K., Yuan, X.Z., Roß-Nickoll, M., Schäffer, A., Hollert, H.,
521 2015. Yangtze Three Gorges Reservoir, China: a holistic assessment of organic
522 pollution, mutagenic effects of sediments and genotoxic impacts on fish. J.
523 Environ. Sci. 38, 63-82.
524 Finizio, A., Mackay, D., Bidleman, T., Harner, T., 1997. Octanol-air partition coefficient
525 as a predictor of partitioning of semi-volatile organic chemicals to aerosols. Atmos.
526 Environ. 31, 2289-2296.
527 Goss, K.U., Schwarzenbach, R.P., 1998. Gas/solid and gas/liquid partitioning of organic
528 compounds: Critical evaluation of the interpretation of equilibrium constants.
529 Environ. Sci. Technol. 32, 2025-2032.
530 Harner, T., Bidleman, T.F., 1998. Octanol-air partition coefficient for describing
531 particle/gas partitioning of aromatic compounds in urban air. Environ. Sci. Technol.
532 32, 1494-1502.
533 Hu, H.L., Tian, M., Zhang, L.M., Yang, F.M., Peng, C., Chen, Y., Shi, G.M., Yao, X.J.,
534 Jiang, C.T., Wang, J., 2019. Sources and gas-particle partitioning of atmospheric
535 parent, oxygenated, and nitrated polycyclic aromatic hydrocarbons in a humid city
536 in southwest China. Atmos. Environ. 206, 1-10.
537 Huang, W.M., Bi, Y.H., Hu, Z.Y., Zhu, K.X., Zhao, W., Yuan, X.G. 2015. Spatio-
538 temporal variations of GHG emissions from surface water of Xiangxi River in
539 Three Gorges Reservoir region, China. Ecol. Eng. 83, 28-32.

Huang, Y.P., Liu, M., Wang, R.Q., Khan, S.K., Gao, D.Z., Zhang, Y.Z., 2017. Characterization and source apportionment of PAHs from a highly urbanized river sediments based on land use analysis. Chemosphere, 184, 1334-1345.

Jenkins, B.M., Jones, A.D., Turn, S.Q., Williams, R.B., 1996. Particle concentrations, gas-particle partitioning, and species inter-correlations for polycyclic aromatic hydrocarbons (PAH) emitted during biomass burning. Atmos. Environ. 30, 3825-3835.

Jia, J.P., Deng, L., Bi, C.J., Jin, X.P., Zeng, Y.S., Chen, Z.L., 2021. Seasonal variations, gas-PM2.5 partitioning and long-distance input of PM2.5-bound and gas-phase polycyclic aromatic hydrocarbons in Shanghai, China. Atmos. Environ. 252, 118335.

Jiang, Y.F., Hu, X.F., Yves, U.J., Zhang, H.Y., Wu, Y.Q., 2014. Status, Source and health risk assessment of polycyclic aromatic hydrocarbons in street dust of an industrial city, NW China. Ecoto. Environ. Safe. 106(0): 11-18.

Jiang, Y.Q., Lin, T., Wu, Z.L., Li, Y.Y., Li, Z.X., Guo, Z.G., Yao, X.H., 2018a. Seasonal atmospheric deposition and air-sea gas exchange of polycyclic aromatic hydrocarbons over the Yangtze River Estuary, East China Sea: Implications for source-sink processes. Atmos. Environ. 178, 31-40.

Jiang, T., Wang, D.Y., Wei, S.Q., Yan, J.L., Liang, J., Chen, X.S., Liu, J., Wang, Q.L., Lu, S., Gao, J., 2018b. Influences of the alternation of wet-dry periods on the variability of chromophoric dissolved organic matter in the water level fluctuation zone of the Three Gorges Reservoir area, China. Sci. Total Environ. 636, 249-259.

562 Kim, S.K., Chae, D.H., 2016. Seasonal variation in diffusive exchange of polycyclic
563 aromatic hydrocarbons across the air-seawater interface in coastal urban area. Mar.
564 Pollut. Bull. 109, 221-229.
565 Lao, J.Y., Li, T.Y., Wu, R.B., Ruan, Y.F., Zeng, E.Y., Wu, J.X., Lam, P.K.S., 2021.
566 Tracing human footprint and the fate of atmospheric polycyclic aromatic
567 hydrocarbons over the Pearl River Estuary, China: Importance of particle size. Sci.
568 Total Environ. 767, 144267.
569 Li, C.C., Huo, S.L., Yu, Z.Q., Xi, B.D., Yeager, K.M., He, Z.S., Ma, C.Z., Zhang, J.T.,
570 Wu, F.C., 2017. National investigation of semi-volatile organic compounds (PAHs,
571 OCPs, and PCBs) in lake sediments of China: Occurrence, spatial variation and
572 risk assessment. Sci. Total Environ. 579, 325-336.
573 Li, J., Cheng, H.R, Zhang, G., Qi, S.H., Li, X.D., 2009. Polycyclic aromatic
574 hydrocarbon (PAH) deposition to and exchange at the air–water interface of Luhu,
575 an urban lake in Guangzhou, China. Environ. Pollut. 157, 273-279.
576 Liu, Y., Wang, S.Y., Mcdonough, C.A., Khairy, M., Muir, D.C.G., Helm, P.A., Lohmann,
577 R., 2016. Gaseous and freely-dissolved PCBs in the lower great lakes based on
578 passive sampling: Spatial trends and air-water exchange. Environ. Sci. Technol.
579 50, 4932-4939.
580 Lohmann, R., Harner, T., Thomas, G.O., Jones, K.C., 2000. A comparative study of the
581 gas-particle partitioning of PCDD/Fs, PCBs, and PAHs. Environ. Sci. Technol. 34,
582 4943-4951.
583 McDonough, C.A., Khairy, M.A., Muir, D.C.G., Lohmann, R., 2014. Significance of

584 population centers as sources of gaseous and dissolved PAHs in the lower Great
585 Lakes. Environ. Sci. Technol., 48, 7789-7797.
586 McDonough, C.A., Puggioni, G., Helm, P.A., Muir, D., Lohmann, R., 2016. Spatial
587 distribution and air-water exchange of organic flame retardants in the lower Great
588 Lakes. Environ. Sci. Technol. 50, 9133-9141.
589 Na, G.S., Ye, J.D., Li, R.J., Gao, H., Jin, S.C., Gao, Y.Z., Hou, C., Huang, J.J., 2021.
590 Fate of polycyclic aromatic hydrocarbons in the Pacific sector of the Arctic Ocean
591 based on a level III fugacity environmental multimedia model. Mar. Pollut. Bull.
592 166, 112195.
593 Nelson, E. D., Mcconnell, L. L., Baker, J. E. 1998. Diffusive exchange of gaseous
594 polycyclic aromatic hydrocarbons and polychlorinated biphenyls across the air-
595 water interface of the Chesapeake Bay. Environ. Sci. Technol. 32, 912-919.
596 Odabasi, M., Cetin, E., Sofuoglu, A., 2006. Determination of octanol-air partition
597 coefficients and supercooled liquid vapor pressures of PAHs as a function of
598 temperature: Application to gas-particle partitioning in an urban atmosphere.
599 Atmos. Environ. 40, 6615-6625.
600 Pankow, J.F., 1994. An absorption-model of gas-particle partitioning of organic-
601 compounds in the atmosphere. Atmos. Environ. 28, 185-188.
602 Ravindra, K., Sokhi, R., Grieken, R.V., 2008. Atmospheric polycyclic aromatic
603 hydrocarbons: Source attribution, emission factors and regulation. Atmos. Environ.
604 42(13): 2895-2921.
605 Ruge, Z., Muir, D., Helm, P., Lohmann, R., 2015. Concentrations, trends, and air-water

606 exchange of PAHs and PBDEs derived from passive samplers in Lake Superior in
607 2011. Environ. Sci. Technol., 49, 13777-13786.
608 Schwarzenbach, R.P., Gschwend, P.M., Imboden, D.M., 2003. Environmental Organic
609 Chemistry, second ed. Wiley, Hoboken, USA, pp. 906-937.
610 Shoemaker, D.P., Garland, G.W., Steinfeld, J.I., 1974. Propagation of errors.
611 Experiments in physical chemistry (pp. 51–58). New York, NY: McGraw-Hill.
612 Simcik, M.F., Eisenreich, S.J., Lioy, P.J., 1999. Source apportionment and source/sink
613 relationships of PAHs in the coastal atmosphere of Chicago and Lake Michigan.
614 Atmos. Environ. 33, 5071-5079.
615 Simcik, M.F., Franz, T.P., Zhang, H.X., Eisenreich, S.J., 1998. Gas-particle partitioning
616 of PCBs and PAHs in the Chicago urban and adjacent coastal atmosphere: States
617 of equilibrium. Environ. Sci. Technol. 32, 251-257.
618 Sitaras, L.E., Bakeas, E.B., Siskos, P.A., 2004. Gas/particle partitioning of seven
619 volatile polycyclic aromatic hydrocarbons in a heavy traffic urban area. Sci. Total
620 Environ. 327, 249-264.
621 Tao, Y.Q., Yu, J., Lei, G.L., Xue, B., Zhang, F.J., Yao, S.C., 2017. Indirect influence of
622 eutrophication on air-water exchange fluxes, sinking fluxes, and occurrence of
623 polycyclic aromatic hydrocarbons. Water Res. 122, 512-525.
624 Terzi, E., Samara, C., 2004. Gas-particle partitioning of polycyclic aromatic
625 hydrocarbons in urban, adjacent coastal, and continental background sites of
626 western Greece. Environ. Sci. Technol. 38, 4973-4978.
627 Tucca, F., Luarte, T., Nimptsch, J., Woelfl, S., Pozo, K., Casas, G., Dachs, J., Barra, R.,

628 Chiang, G., Galban-Malagon, C., 2020. Sources and diffusive air-water exchange
629 of polycyclic aromatic hydrocarbons in an oligotrophic North-Patagonian lake. Sci.
630 Total Environ. 738, 139838.
631 Verma, K.P., Sah, D., Kumari, K.M., Lakhani, A., 2017. Atmospheric concentrations
632 and gas–particle partitioning of polycyclic aromatic hydrocarbons (PAHs) and
633 nitro-PAHs at Indo-Gangetic sites. Environ. Sci.: Processes Impacts, 19, 1051-
634 1060.
635 Wania F., Axelman, J., Broman, D., 1998. A review of processes involved in the
636 exchange of persistent organic pollutants across the air-sea interface. Environ.
637 Pollut. 102(1), 3-23.
638 Wang, J.X., Bi, Y.H., Pfister, G., Henkelmann, B., Zhu, K.X., Schramm, K.W., 2009.
639 Determination of PAH, PCB, and OCP in water from the Three Gorges Reservoir
640 accumulated by semipermeable membrane devices (SPMD). Chemosphere, 75(8):
641 1119-1127.
642 Wang, X., Wang, F.W., Feng, T., Zhang, S.Y., Guo, Z.G., Lu, P.L., Liu, L., Yang, F.M.,
643 Liu, J.X., Rose, N.L., 2020. Occurrence, sources and seasonal variation of PM2.5
644 carbonaceous aerosols in a water level fluctuation zone in the Three Gorges
645 Reservoir, China. Atmos. Pollut. Res. 11, 1249-1257.
646 Wang, Z., Na, G.S., Ma, X.D., Fang, X.D., Ge, L.K., Gao, H., Yao, Z.W., 2013.
647 Occurrence and gas/particle partitioning of PAHs in the atmosphere from the
648 North Pacific to the Arctic Ocean. Atmos. Environ. 77, 640-646.
649 Wolf, A., Bergmann, A., Wilken, R.D., Gao, X., Bi, Y.H., Chen, H., Schuth, C., 2013.

Occurrence and distribution of organic trace substances in waters from the Three Gorges Reservoir, China. Environ. Sci. Pollut. Res. 20(10): 7124-7139.

Wu, X.W., Wang, Y., Zhang, Q.N., Zhao, H.X., Yang, Y., Zhang, Y.W., Xie, Q., Chen, JW., 2019. Seasonal variation, air-water exchange, and multivariate source apportionment of polycyclic aromatic hydrocarbons in the coastal area of Dalian, China. Environ. Pollut. 244, 405-413.

Wu, Z.L., Lin, T., Li, Z.X., Jiang, Y.Q., Li, Y.Y., Yao, X.H., Gao, H.W., Guo, Z.G., 2017. Air-sea exchange and gas-particle partitioning of polycyclic aromatic hydrocarbons over the northwestern Pacific Ocean: Role of East Asian continental outflow. Environ. Pollut. 230, 444-452.

Ye, C., Li, S.Y., Zhang, Y.L., Zhang, Q.F., 2011. Assessing soil heavy metal pollution in the water-level-fluctuation zone of the Three Gorges Reservoir, China. J. Hazard. Mater. 191, 366-372.

Yue, J.S., Yuan, X.Z., Li, B., Ren, H.Q., Wang, X.F., 2016. Emergy and exergy evaluation of a dike-pond project in the drawdown zone (DDZ) of the Three Gorges Reservoir (TGR). Ecol. Indic. 71, 248-257.

Zakaria, M.P., Takada, H., Tsutsumi, S., Ohno, K., Yamada, J., Kouno, E., Kumata, H., 2002. Distribution of Polycyclic Aromatic Hydrocarbons (PAHs) in Rivers and Esuaries in Malaysia: A Widespread Input of Petrogenic PAHs. Environ. Sci. Technol. 36(9): 1907.

Zhang, K., Gong, W., Lv, J.Z., Xiong, X., Wu, C.X., 2015. Accumulation of floating microplastics behind the Three Gorges Dam. Environ. Pollut. 204, 117-123.

672 Zhang, R.J., Han, M.W., Yu, K.F., Kang, Y.R., Wang, Y.H., Huang, X.Y., Li, J., Yang,
673 Y., 2021a. Distribution, fate and sources of polycyclic aromatic hydrocarbons
674 (PAHs) in atmosphere and surface water of multiple coral reef regions from the
675 South China Sea: A case study in spring-summer. J. Hazard. Mater. 412, 125214.
676 Zhang, X., Zhang, Z.F., Zhang, X.M., Yang, P.F., Li, Y.F., Cai, M.H., Kallenborn, R.,
677 2021b. Dissolved polycyclic aromatic hydrocarbons from the Northwestern
678 Pacific to the Southern Ocean: Surface seawater distribution, source
679 apportionment, and air-seawater exchange. Water Res.117780.
680 Zhang, Y.F., Song, Y.G., Tian, J., Zhao, H.B., Yang, S., Wu, J.B., 2018. Occurrence and
681 Gas-particle Partitioning of Polycyclic Aromatic Hydrocarbons in the Air of
682 Liaodong Bay. Environ. Sci. 39, 1527-1536 (in Chinese).
683
684
685
686
687
688
689
690